Check for updates

JGR Atmospheres

RESEARCH ARTICLE
10.1029/2021JD034857

Uncertainty of Tropical Cyclone Wind Radii on Sea Surface Temperature Cooling

Iam-Fei Pun[1], John A. Knaff[2], and Charles R. Sampson[3]

[1]Graduate Institute of Hydrological and Oceanic Sciences, National Central University, Taoyuan, Taiwan, [2]NOAA Center for Satellite Applications and Research, Fort Collins, CO, USA, [3]Naval Research Laboratory, Monterey, CA, USA

Key Points:

- TC wind radii analyses and forecasts from operational Joint Typhoon Warning Center forecast and Hurricane Weather Research and Forecasting model contain various degrees of uncertainty
- Uncertainty of wind radii can lead to a significant error in sea surface temperature (SST) cooling estimation
- The correlation between SST cooling and tropical cyclone size is highest among all the parameters tested in this study

Correspondence to:
I.-F. Pun,
ipun@ncu.edu.tw

Citation:
Pun, I.-F., Knaff, J. A., & Sampson, C. R. (2021). Uncertainty of tropical cyclone wind radii on sea surface temperature cooling. *Journal of Geophysical Research: Atmospheres*, *126*, e2021JD034857. https://doi.org/10.1029/2021JD034857

Received 5 MAR 2021
Accepted 23 JUN 2021

© 2021. American Geophysical Union. All Rights Reserved.

Abstract The sea surface temperature (SST) beneath a tropical cyclone (TC) is of great importance to its dynamics; therefore, understanding and accurately estimating the magnitude of SST cooling is of vital importance. Existing studies have explored important influences on SST of TC translation speed, maximum surface winds, ocean thermal condition, and ocean stratification. But the influence of the TC wind radii (or collectively called the TC size) on SST has been largely overlooked. In this study, we assess the influence of wind radii uncertainty on SST cooling by a total of 15,983 numerical simulations for the western North Pacific during the 2014–2018 seasons. Results show a 6%–20% SST cooling error induced using wind radii from the Joint Typhoon Warning Center official forecast and a 35%–40% SST cooling error using wind radii from the operational runs of the Hurricane Weather Research and Forecasting (HWRF) model. Our results indicate that SST cooling is most sensitive to the radius of 64 kt winds (R64) due to its effects on the integrated kinetic energy of the TC and subsequent mixing of the ocean surface layer. It is also found that the correlation between SST cooling induced by the TC and its size is 0.49, which is the highest among all the parameters tested. This suggests that it is extremely important to get TC size correct in order to predict the SST cooling response, which then impacts TC evolution in numerical weather prediction models.

1. Introduction

Tropical cyclones (TCs) in the western North Pacific are some of the most destructive natural disasters on Earth (Emanuel, 2020; Lin et al., 2014, 2021; Peduzzi et al., 2012; Pun et al., 2019). Typhoons, which are TCs with winds greater than 64 kt (1 kt = 0.514 ms^{-1}) and occur in the western North Pacific, can be especially devastating when making landfall. With increasing Asian and western Pacific population and economic prosperity, coastal areas are becoming more vulnerable to typhoons (e.g., Emanuel, 2020; Potter et al., 2019; Pun et al., 2019), and changes in climate such as sea level rise will only increase that vulnerability. The most effective way to mitigate TC damage and save expensive assets, is to increase TC prediction skill so that appropriate pre-storm preparations are completed in a timely manner. Unfortunately, increasing skill has proven to be difficult. Enormous efforts in the past few decades have led to improvements in TC track prediction, but intensity prediction skill is still limited, especially in the cases of rapid intensification (RI; Bender et al., 2019; Cangialosi et al., 2020; DeMaria et al., 2014; Rappaport et al., 2012; Rogers et al., 2017). Much of the issue with intensity forecasting skill can be attributed to complex interactions between internal dynamics, TC structure, and surrounding air-sea environments (Emanuel, 1999; Kaplan et al., 2015; Wang & Wu, 2004).

From an energy supply perspective, the sea surface temperature (SST) directly beneath the TC's inner core is critical to subsequent TC intensity change (e.g., Balaguru et al., 2015; Emanuel, 1999; Jaimes et al., 2015; Lin et al., 2008, 2009, 2013; Pun et al., 2018, 2019; Shay et al., 2000; Zhang et al., 2017). Strong winds associated with TCs act to mix the upper ocean and entrain colder water from below, reducing the temperature of the surface layer (Price, 1981). As a result, the TC initiates self-induced SST cooling (Black et al., 2007; D'Asaro et al., 2014; Lin et al., 2005; Price, 1981; Sanford et al., 2007; Yang et al., 2019). Emanuel (1999) suggested that even a few degree of SST cooling would be sufficient to cut off the energy supply from the ocean as the heat flux approaches zero. Therefore, providing an accurate self-induced SST cooling estimate is key to improving TC intensity prediction (Emanuel, 1999; Hong et al., 2000; Lin et al., 2005, 2008; 2013; Mei et al., 2015; Wu et al., 2016). The magnitude of SST cooling is strongly related to TC's characteristics and upper ocean conditions (D'Asaro et al., 2014; Glenn et al., 2016; Lin et al., 2008, 2009; Price, 1981; Shay

& Brewster, 2010; Shay et al., 2000). Past studies have generally explored effects of ocean thermal structure (e.g., Ford et al., 2020; Huang et al., 2015; Knaff et al., 2013; Lin et al., 2005, 2008; Shay et al., 2000) and TC translation speed (e.g., Chang et al., 2020; Lin et al., 2009; Mei et al., 2012). Others have investigated the role of salinity-induced ocean stratification in SST cooling (e.g., Balaguru et al., 2015, 2020; Shay & Brewster, 2010) and the role of enthalpy fluxes (Cione & Uhlhorn, 2003). However, TC size has received less attention, even though it has been identified as a controlling factor in SST change (D'Asaro et al., 2014; Lin et al., 2021; Knaff et al., 2013; Potter et al., 2019; Price, 1981).

TC size is closely correlated to the forcing time, the time that wind of a certain magnitude blows over a specific point in the ocean. Based on synoptic wind radii information, Pun et al. (2018) found that the drastic size change in Super Typhoon Megi (2010) was partially responsible for intense SST cooling (~7°C) Typhoon Megi generated in the South China Sea. Their results emphasized how TC size can be as impactful as translation speed in determining SST cooling. Based on the limited results in Pun et al. (2018) and a few other studies (e.g., Bender et al., 2017; Tallapragada et al., 2014; Zhang et al., 2019), the authors postulate that it is vital to better understand how TC size affects ocean cooling.

TC wind radii have been estimated with varying degrees of accuracy for decades (see Chu et al., 2002; Landsea & Franklin, 2013; Sampson et al., 2017). Such information is used in practical applications such as wind speed probability forecasts, wave and storm surge forecasting, and evacuation planning (DeMaria et al., 2013; Powell & Reinhold, 2007; Sampson et al., 2010, 2012). However, the wind radii (collectively referred in this work as TC size) are difficult to both observe and simulate since they are continually affected by environmental factors and TC motion (Chan and Chan, 2012, 2013; Hill & Lackmann, 2009; Mok et al., 2018). Even with recently available satellite imagery techniques, the observational uncertainty in TC size is still an issue (Combot et al., 2020; Knaff & Sampson, 2015; Landsea & Franklin, 2013; Reul et al., 2017). Many studies have devoted efforts to discuss uncertainty with and improvement in estimates of TC wind radii (e.g., Knaff & Sampson, 2015; Landsea & Franklin, 2013; Sampson et al., 2018), but issues still exist (Sampson & Knaff, 2015; Sampson et al., 2017, 2018).

In this study, we assess wind radii/TC size uncertainty from two well-established sources for the western North Pacific during 2014–2018. We then evaluate the potential SST cooling errors induced by wind radii uncertainty based on a large number of numerical simulations. The data and method are discussed in Section 2. Our results, which indicate that the magnitude of SST cooling is closely linked to TC size, are presented in Section 3. Finally, we present a discussion on this topic and make conclusions based on our results in Sections 4 and 5, respectively.

2. Data and Method

2.1. TC Wind Radii

TC surface winds can be characterized by the maximum radial extent of three wind speeds: 34 kt (R34), 50 kt (R50), and 64 kt (R64). In operations, these are typically referred to as "the wind radii". Following Pun et al. (2018), these three sets of wind radii are collectively defined herein as "TC size". For our study, real-time analysis (i.e., 0 h) and forecasts (i.e., 12, 24, 36, 48, and 72 h) of the wind radii are extracted from the forecast records contained in the Automated Tropical Cyclone Forecasting System (Sampson & Schrader, 2000). These comprehensive data files are archived on the collaboration site of the US Joint Typhoon Warning Center (JTWC; https://pzal.metoc.navy.mil). The wind radii are provided at 6-hourly intervals in four compass quadrants (i.e., northeast, southeast, southwest, and northwest), collected from a variety of forecast centers and models. This study uses two operational forecast data sets: JTWC official forecast and operational Hurricane Weather Research and Forecasting (HWRF) model forecasts. Hereafter, these two data sets are referred to Joint Typhoon Warning Center official forecast (JTWCO) and operational Hurricane Weather Research and Forecasting model (HWRFO), respectively. While most JTWCO and HWRFO forecasts extend to 120 h, our study's assessment focuses on the 0–72 h period, and forecasts times 0, 12, 24, 36, 48, and 72 h, which insures large and meaningful sample sizes.

To evaluate analysis and forecast errors, we use wind radii from the final JTWC best track database as ground truth. Although there may be some inherent issues regarding the quality of best track wind radii (Knaff & Sampson, 2015; Landsea & Franklin, 2013), the best track data set currently provides the most reliable and homogeneous wind radii reanalysis. To ensure the highest quality best track wind radii infor-

mation, the period of study is 2014–2018, which corresponds with JTWC's transition into quality control and post-season assessment of best track wind radii (Sampson et al., 2017). JTWC's best tracks are available at https://www.metoc.navy.mil/jtwc/jtwc.html.

2.2. Ocean Temperature Profiles

In order to estimate the SST cooling, this study uses gridded monthly Argo data (Roemmich & Gilson, 2009) to provide initial ocean temperature profiles for our numerical simulations. Taking advantage of high-quality temperature measurements from the global Argo array (Argo Science Team, 2000), this data set regularly generates monthly temperature and salinity fields for the upper 2,000 m at 1° × 1° horizontal resolution (Roemmich & Gilson, 2009). The vertical resolution varies, with finer spacing (on the order of 10 m) in the near surface layer to a depth of 200 m. The upper 200 m in the ocean is where the most intense TC-ocean interaction takes place (Lin et al., 2005, 2013, 2014; Pun et al., 2018, 2019; Sanford et al., 2007; Shay et al., 2000; Wu et al., 2016; Yang et al., 2019). For each TC location, the corresponding temperature profile is extracted based on closest 1° grid box and month. This profile will be used to initialize the ocean model. Note that TC trajectories in this study are based on JTWC best track data. That is, forecasted TC parameters from JTWCO and HWRFO are relocated to JTWC best track positions. More details in numerical settings will be introduced in next section. The Argo data set can be downloaded from http://sio-argo.ucsd.edu/RG_Climatology.html.

2.3. Three-Dimensional Price-Weller-Pinkel Ocean Model (3DPWP)

We use the three-dimensional Price-Weller-Pinkel Ocean Model (3DPWP) ocean model to evaluate the sensitivity of TC-induced SST cooling to TC size. The 3DPWP is a realistic deep ocean model designed for studying upper ocean response to surface forcing and is particularly appropriate for modeling a moving TC (Price et al., 1994). The momentum, temperature, and salinity budgets in the 3DPWP are all based on primitive equations. Wind-driven vertical mixing is implemented through the parameterization by considering static stability, vertical entrainment and instability due to vertical shear flows. In all, the 3DPWP contains the primary processes controlling SST cooling during a TC passage – vertical mixing, upwelling, horizontal advection, and air-sea heat exchange. The 3DPWP has been widely used and proven to be successful for investigating the ocean response to a TC (e.g., Balaguru et al., 2015; Guan et al., 2014; Lin et al., 2013, 2014, 2021; Pun et al., 2018; Sanford et al., 2007; Walker et al., 2014). In an effort to advance TC intensity simulations and predictions, the 3DPWP has even been coupled with the Weather Research and Forecasting (WRF) atmospheric numerical weather prediction model to improve ocean representation (Chen et al., 2007; Wu et al., 2016).

Figure 1 shows an example of how an idealized individual case is initialized (left) and a simulation result (right). The 3DPWP spatial domain extends 400 km from the TC center in the across TC track direction, and 690 km in the along-track direction and a horizontal resolution of 5 km. There are 45 vertical layers at intervals of 5-, 10-, and 50-m in the 0–100, 100–200, and 200–1,000 m depth layers, respectively. The entire domain contains 161 across ×277 along ×45 vertical grid points. The temperature field is homogeneously initialized with the corresponding temperature profile extracted from the monthly Argo data set (Figure 1a). The 3DPWP has neither bathymetry nor terrain, and salinity is held constant to 35 psu. Ocean currents are also initialized at zero, then allowed to spin up throughout the model integration. An example of a 3DPWP simulation is shown in Figure 1b, where the *y*-direction is along the track and the *x*-direction is across the track. The TC translation speed is calculated from two adjacent 6-hourly best track positions. Following Pun et al. (2018), the TC wind field input to the model is axisymmetric and constructed from the TC's characteristics: maximum wind speed (V_{max}), radius of maximum wind (RMW) and three wind radii. For simplicity, R34, R50, and R64 are constructed by averaging non-zero values of the four quadrants of the wind radii (Figure 1). To start the integration, the TC is initially located a distance of one R34 below the *x*-axis (Figure 1a). The model evolves every 600 s for a distance of twice the R34 (Figure 1b). The magnitude of the resultant SST cooling for each TC case is defined as the lowest temperature along the *x*-axis.

All six-hourly over-ocean TC best track positions in the western North Pacific domain (5–30°N, 121–180°E) and the South China Sea domain (5–24°N, 105–121°E) are considered for 3DPWP simulations (Figure 2a).

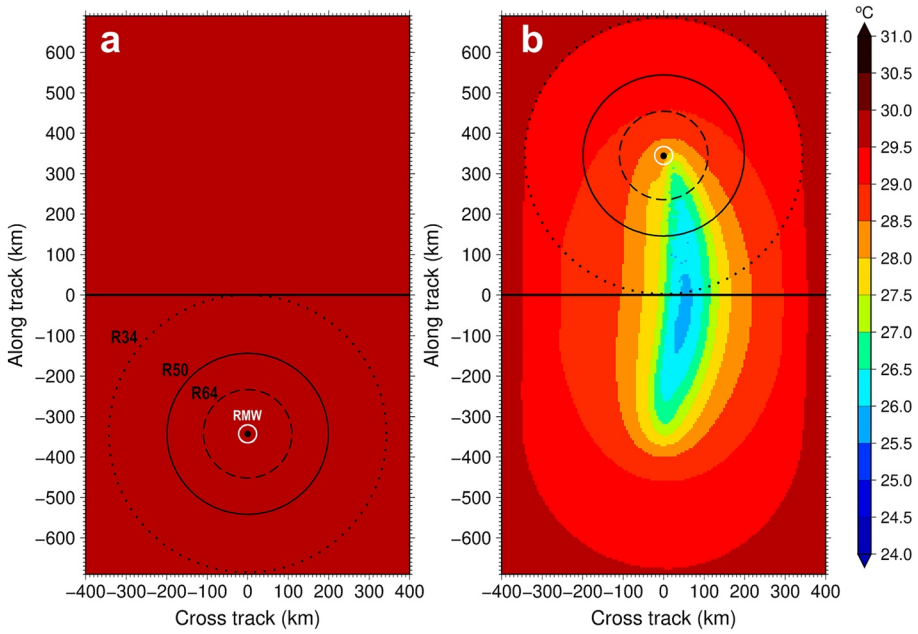

Figure 1. An idealized example of one three-dimensional Price-Weller-Pinkel Ocean Model simulation case at (a) initial stage and (b) final stage. The black circles indicate the size of R34, R50 and R64. The black dot and white circle indicate the tropical cyclone (TC) center and radius of maximum wind, respectively. The initial ocean structure is horizontally homogeneous based on monthly Argo gridded data. In the model, the TC is moving upward with observed translation speed. The resulted sea surface temperature (SST) cooling is obtained as compared to the initial SST. In this exemplary case, V_{max} is 170 kt, while translation speed is 6 m s^{-1}.

However, cases are limited to those (a) evolving in deep water regions where Argo profiles are available, and (b) TCs with R34 wind radii estimates. These restrictions result in 1,765 cases (yellow dots in Figure 2a).

Three groups of simulations, totaling 15,983 runs, are conducted to assess SST cooling sensitivity to TC size (Table 1). The first group (control) is all based on JTWC best track TC information (i.e., TC location, V_{max}, RMW, wind radii, and translation speed). The results from the first group are used as a baseline to assess the impact of different TC size on SST cooling. The second and third groups are experiments in which the best track wind radii are replaced with analysis and forecast wind radii from the JTWC (JTWCO) and HWRF (HWRFO), respectively. The JTWCO and HWRFO groups each have one analysis and five forecast periods. In these simulations, a monthly Argo temperature profile under each TC location is used to initialize the 3DPWP model, and then SST cooling is simulated. Again, the only differences among these simulation sets are the TC wind radii (i.e., R34, R50, and R64). Other variables such as TC location, V_{max}, RMW, translation speed, and initial ocean temperature structure are the same as in the control group. In doing so, differences in resultant cooling are only due to differences in TC size estimates.

3. Results

3.1. Wind Radii Uncertainty in Operational Data Sets

We first examine the performance of the operational wind radii estimated by JTWCO and HWRFO. In order to obtain meaningful comparisons, a homogeneous set for each time step is generated. That is, TC cases are considered only when JTWCO and HWRFO are both available. Figure 3 shows the mean absolute errors based on the JTWC best track ground truth during 2014–2018 (here after referred to as the "errors", if not indicated otherwise) for the three wind radii estimates for the analysis (0 h) and forecast fields (12–72 h). JTWCO wind radii errors are generally larger for R34 than for R50, and larger for R50 than for R64. This is to be expected as the weaker wind (i.e., 34 kt) has a much larger radius, and the wind speed increases exponentially toward the TC center until reaching the RMW (D'Asaro et al., 2014; Holland et al., 2010; Pun et al., 2018; Wang & Wu, 2004). At the 12-h forecast time, JTWCO R34, R50, and R64 errors and standard

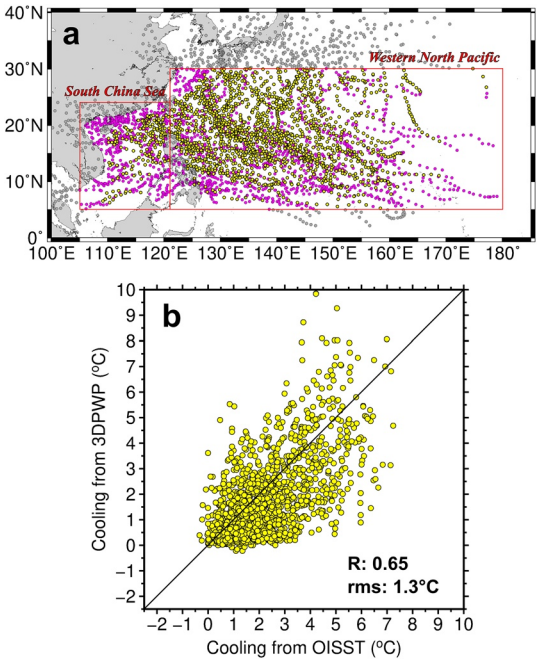

Figure 2. (a) 6-h track points for all tropical cyclones from 2014 to 2018 in Joint Typhoon Warning Center best track data set. Pink dots indicate the over-ocean cases over the western North Pacific and South China Sea (red boxes). There are 1,765 valid cases for three-dimensional Price-Weller-Pinkel Ocean Model (3DPWP) simulations (yellow dots) that match Argo profiles. Gray dots indicate the cases over land or outside the study area. (b) Sea surface temperature (SST) cooling comparison between the 3DPWP simulations and satellite Optimal Interpolated estimates for cases in (a) with correlation coefficient (R) and root mean square difference.

deviation of the errors are 31.8 ± 31.0, 20.7 ± 23.5, and 14.0 ± 13.2 km, respectively (blue curves in Figure 3). HWRFO R34 errors are larger than the R50 errors, but the R50 errors are slightly smaller than the R64 errors (green curves in Figure 3). Also shown in the graph is the percent error relative to the radii (bars in Figure 3). In contrast to the absolute errors, the error percentages for both JTWCO and HWRFO generally increase toward the center of the TC. From 0 to 72 h, the error percentages for JTWCO are 5%–18%, 5%–24%, and 6%–30% for R34, R50, and R64, respectively. The HWRFO error percentages increase from 29%–37% for R34, to 31%–38% for R50, to 58%–70% for R64. The HWRFO R64 error percentages are nearly double those of its R34.

The analysis field (0 h) is often used as an initial condition for model simulations, and directly impacts model performance (Bender et al., 2017, 2019; Tallapragada et al., 2014). As shown in Figure 3, it is found that JTWCO provides the best wind radii analysis in the present comparison, with the errors and standard deviation of the errors of 10.8 ± 23.0, 6.9 ± 16.9, and 4.2 ± 10.6 km for R34, R50, and R64, respectively. It is equivalent to merely ~5% error with respect to the best track. This is not surprising since JTWC (JTWCO) has access to many observations in near real-time (Sampson et al., 2017), and that many of the same observations are the basis for JTWC's post season or best track analysis. The errors in JTWCO forecasts experience a significant jump from the analysis to 12 h, and generally increase gradually thereafter. The HWRFO analysis errors are much larger than those of JTWCO, and forecast errors appear to drop slightly by the 12-h forecast. This suggests vortex instability in initialization due to use of JTWC's initial TC estimates (Tallapragada et al., 2014). The HWRFO forecast errors then climb gradually to 72 h. Note that the error differences between JTWCO and HWRFO are statistically significant at 99% based on the z-test (a t-test with known standard deviations).

JTWCO has nearly no bias for the three wind radii at all forecast time steps, with the mean bias around ±5 km (blue in Figure 4). The R34 and R64 estimated from JTWCO tend to be slightly underestimated initially, but become somewhat overestimated later in the forecasts, especially at 48 and 72 h. Interestingly, R50 estimated from JTWCO does not have such behavior and tends to have a low bias at all times. In HWRFO, the TC structure is generally larger than observed with positive biases (green in Figure 4). As with the mean absolute errors in Figure 3, the largest biases are associated with the analysis field of HWRFO. Moreover, the degree of the bias varies considerably among the three wind radii. The overall biases (0–72 h) in R34, R50, and R64 estimated from HWRFO are about +52, +24, and +35 km, respectively. On average, HWRFO overestimated the TC size in the western North Pacific for the study period 2014–2018. Modeling TC size is still challenging, even with improvements of model physics initialization and resolution in the operational HWRF system (Bender et al., 2019; Tallapragada et al., 2014).

3.2. SST Cooling Error Induced by Wind Radii Uncertainty

SST cooling can be estimated for each TC track position (hereafter referred to as an individual case) with the 3DPWP. To test the SST sensitivity to wind radii, we use the three TC size data sets discussed above (JTWC best track, JTWCO, and HWRFO) as input to 3DPWP. A total of 13 sets of experiments are conducted in the study. That is, one based on the best track, one based on the operational JTWCO analysis (0 h), one based on the operational HWRFO analysis (0 h), and 5 forecasts (12, 24, 36, 48, and 72 h) for both JTWCO and HWRFO. Table 1 details the number of cases available for the 2014–2018 study period. Again, the only differences between these model cases are the wind radii of R34, R50, and R64, and other variables remain the same, and are based on observed conditions.

Table 1
Case Numbers of 3DPWP Simulations

	2014	2015	2016	2017	2018	Total
JTWC best track (Group 1)						
Best track	277	539	284	259	406	1,765
JTWCO (Group 2)						
0 h	251	486	222	233	324	1,516
12 h	212	419	205	195	281	1,312
24 h	196	413	192	177	273	1,251
36 h	195	396	172	154	235	1,152
48 h	176	349	150	114	203	992
72 h	138	297	110	93	170	808
HWRFO (Group 3)						
0 h	242	456	230	210	312	1,450
12 h	208	417	207	188	281	1,301
24 h	195	400	199	161	272	1,227
36 h	190	373	191	149	256	1,159
48 h	180	369	175	141	229	1,094
72 h	151	323	158	115	209	956

Note. There are three groups: JTWC best track, JTWCO and HWRFO, totaling 15,983 simulations. The only differences in these simulation groups are the R34, R50, and R64.

Abbreviations: 3DPWP, three-dimensional Price-Weller-Pinkel Ocean Model; HWRFO, operational Hurricane Weather Research and Forecasting model; JTWCO, Joint Typhoon Warning Center official forecast; SST, sea surface temperature.

Prior to presenting results against our control group (runs based on the best track), we confirmed the control group SST cooling against observations from the microwave sensor based Optimal Interpolated SST (OISST) data set (Gentemann et al., 2003; Wentz et al., 2000), where we define SST cooling as SST decrease from 7 days before to 1 day after TC passage. In the 1,756 cases evaluated, the 3DPWP simulations generally agree with the OISST results (Figure 2b) with a root mean square difference of 1.3°C and a correlation coefficient (R) = 0.65, which is reasonable given the errors associated with using a simple model like 3DPWP and errors inherent in the OISST analysis.

Figure 5 shows the homogeneous set of 1,391 simulated SST cooling cases for the three analyses. Larger SST cooling tends to occur above the latitude of 17°N and in the South China Sea (Figure 5a), likely due to the shallower mixed layer and colder subsurface ocean condition in those areas (D'Asaro et al., 2014; Ko et al., 2014; Lin et al., 2005; Pun et al., 2018). In addition, it may also be attributed to the TC size and upwelling that tend to increase with latitudes (Chan & Chan, 2015; Mok et al., 2018). Figure 5b shows the cooling differences between the 3DPWP runs with JTWCO analysis and those run with the best track, while Figure 5c shows the same for the HWRFO analysis. Such differences may be more pronounced in Figure 6, which shows the scatter plots for JTWCO and HWRFO respectively versus JTWC in these sets of experiments. As expected, SST cooling changes with different wind radii estimates. The SST cooling driven by JTWCO analysis is comparable to that driven by best track wind radii (Figure 6a). The 5-year mean difference is slightly negative of −0.04°C (SST cooling underestimated), with a standard deviation of 0.23°C. These small differences are expected because JTWCO wind radii are generally similar to the best track wind radii (Figure 6b). The mean differences for the forecast times can be found in Table 2 where we see little biases in the 3DPWP runs with JTWCO. This result is expected as the JTWCO wind radii biases are near zero (Figure 4). On the other hand, SST cooling is clearly more pronounced using wind radii from HWRFO (Figures 5c and 6c). Five-year mean difference is positive, reaching 0.45 ± 0.65°C and is consistent with HWRFO's large positive bias relative to best track wind radii (Figure 6d). From an ocean perspective, this result is consistent with prior research findings that TC residence time increases proportionately with the TC size (Lin et al., 2005; Pun et al., 2018; Price, 1983). In other words, SST cooling is expected to be stronger because the duration of wind forcing is increased, and thus resultant vertical mixing and upwelling are enhanced. Similar outcomes are found for the wind radii in the forecast fields out to 72 h for HWRFO (Table 2).

To assess the SST cooling error from wind radii uncertainty, we produce mean statistics for all time steps from 0 to 72 h (Figure 7). As expected, the lowest SST cooling error is produced using the JTWCO analysis with a mean absolute error and standard deviation of 0.08 ± 0.21°C (Figure 7a). The SST cooling error percentage (based on SST cooling in the best track) with the JTWCO analysis is about 6%. The mean error percentage jumps sharply to 18% at the 12-h forecast, which is expected since the JTWCO wind radii errors also jump sharply (Figure 3). Beyond 12 h, the mean error percentage stabilizes to slightly over 20% (Figure 7a). Although the mean absolute SST cooling error increases with forecast time (curve in Figure 7a), the mean SST cooling in the control group also increases (Table 2) so that the SST cooling error percentage is nearly constant. The HWRFO cooling error (Figure 7b) starts from 0.53 ± 0.58°C, then drops slightly during the first 12 h to 0.51 ± 0.52°C and increases slowly out to 72 h. The magnitude of the reduction in the first 12 h is not as prominent as that of HWRFO wind radii (cf. Figure 3). On the other hand, the 5-year mean cooling error percentage decreases slightly from greater than 40% at 0 h to a minimum error of ∼35% at 36 h, then remains almost constant. The SST cooling error induced by HWRFO analysis wind radii is nearly seven times higher (with a statistical significance of 99%) than that produced by JTWCO analysis wind radii, demonstrating how HWRFO's larger wind radii impact the 3DPWP simulations. This does not prove that

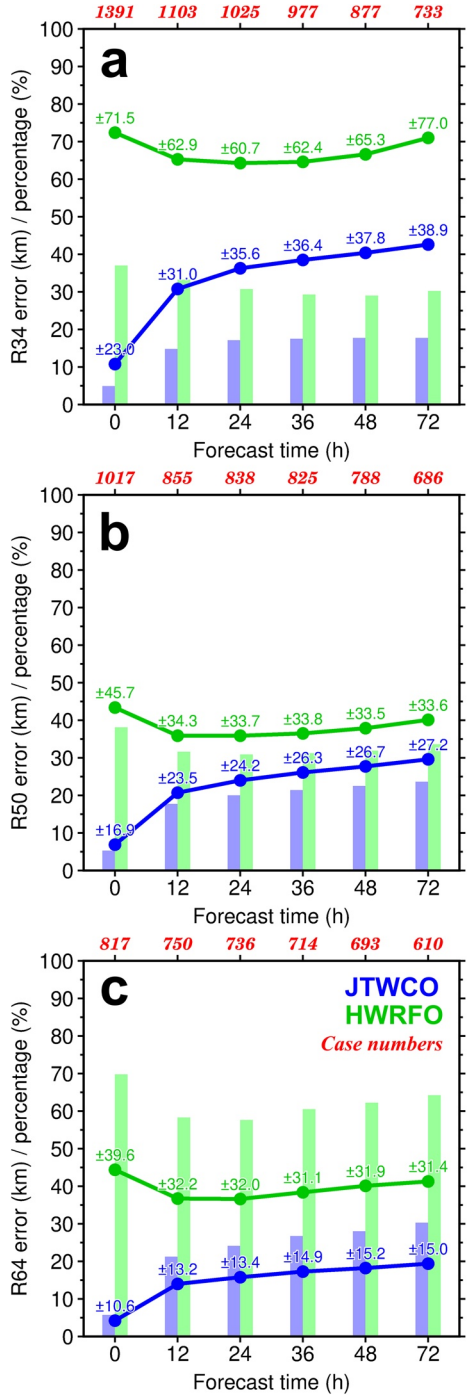

Figure 3. Mean absolute errors (curves), standard deviations (numbers) and error percentages (bars) for estimated (a) R34, (b) R50 and (c) R64 with respect to Joint Typhoon Warning Center (JTWC) best track for 0–72 h. Results of Joint Typhoon Warning Center official forecast (JTWCO) and operational Hurricane Weather Research and Forecasting model (HWRFO) are depicted in blue and green, respectively and the data set at each forecast period is homogeneous. Numbers of cases are shown in red. The error differences between JTWCO and HWRFO are statistically significant at 99% in *z*-tests.

the JTWCO 3DPWP results are more correct, but it does demonstrate just how important TC size can be to SST cooling.

3.3. Case Study of Mangkhut (2018) and Sarika (2016)

The statistics above show characteristics of the means, but variations in individual cases can be dramatic as demonstrated by the Mangkhut (2018) and Sarika (2016) and cases shown in Figures 5b and 5c. Typhoon Mangkhut (2018) had an estimated peak wind speed of 155 kt and was one of the strongest typhoons in 2018 season. The HWRFO analysis overestimates Mangkhut's size, especially near the time of peak intensity at 1800 UTC September 12, 2018 (Figures 8b–8d). R34, R50, and R64 analysis errors of 54%, 123%, and 184%, respectively, with respect to the best track are found near peak intensity. As a result, the corresponding 3DPWP SST cooling is overestimated by 2.4°C (Figure 8a). Such overestimation is critical for TC intensity simulations and predictions because this difference in SST cooling can make a big difference in air-sea energy transfer, especially under the eyewall (Emanuel, 1999; Lin et al., 2013; Pun et al., 2019). In contrast, JTWCO analysis estimates of Mangkhut's wind radii are in good agreement with the best track so that the resultant 3DPWP SST cooling error is within 0.5°C (Figure 8).

The second typhoon case, Sarika (2016), had an estimated peak intensity of 115 kt at 1800 UTC October 15, 2016 as it made landfall in the island of Luzon, Philippines. Sarika exhibited a track similar to Mangkhut, traversing from the western North Pacific to the South China Sea (Figure 5). Unlike in Mangkhut, large wind radii errors are associated with JTWCO's analysis, especially when Sarika re-emerged in the South Chain Sea. JTWCO analysis estimates of R34, R50, and R64 are significantly underestimated by 38%, 48%, and 58%, respectively (Figures 9b–9d). As a result, the simulated SST cooling is simultaneously underestimated by 2.4°C (Figure 9a). This result has a huge implication because it occurs during the time period when Sarika was about to make a second landfall on southern China. The large underestimate of SST cooling may have led to an unrealistic forecast of Sarika's intensity, and thus jeopardized the awareness of the local residents. On the other hand, HWRFO's wind radii are roughly consistent with the best track in this typhoon case. These two contrasting examples further emphasize the importance of wind radii on SST cooling and that there is still considerable uncertainty in both the real-time analyses and best tracks.

3.4. Sensitivity of Individual Wind Radii

The results in previous section demonstrated that the accuracy of the TC-induced SST cooling estimation is closely tied to variations in wind radii and TC size, but the sensitivity analysis did not separate out impacts from the individual wind radii (R34 vs. R50 vs. R64). This topic is further explored here to provide forecasters, modelers and other users a better understanding of how variations of individual wind radii change the 3DPWP ocean model's SST response.

Absolute SST cooling error versus the absolute error associated with each wind radius is performed in this section. 3DPWP results indicate

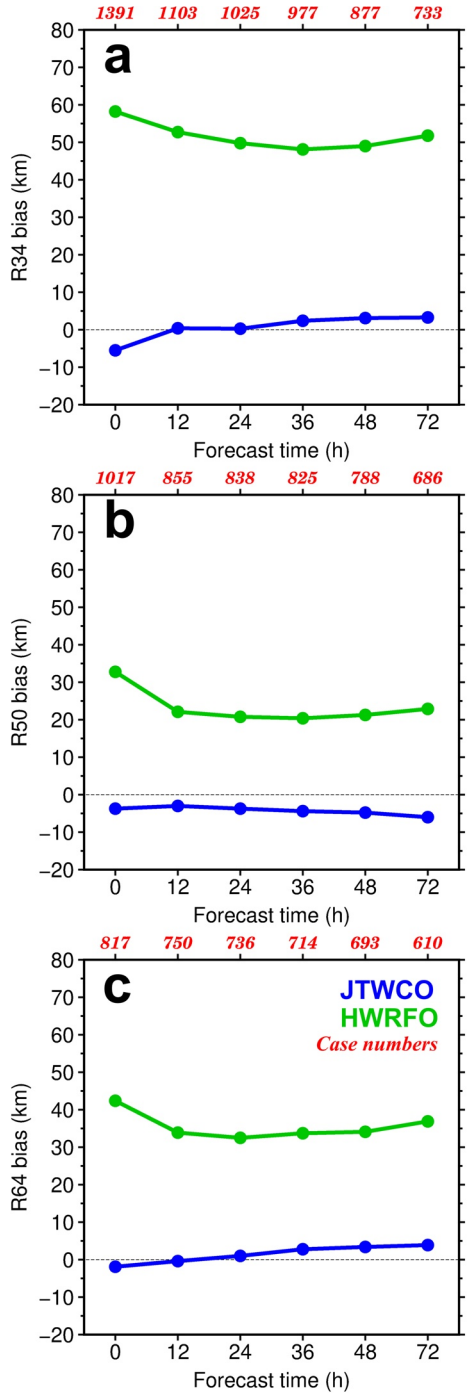

Figure 4. Same as Figure 3, but for the biases.

that SST cooling error in 3DPWP runs with HWRFO analysis is better correlated (R = 0.75) with R64 error than with those from other radii (Figure 10). Correlations are lower when we test sensitivity to R50 (R = 0.66) and R34 (R = 0.50). Analysis of the regression coefficients also reveals that the SST cooling is most sensitive to the change in R64 with a slope of 1.2°C per 100 km. In other words, a 100-km error in R64 is related to a 1.2°C error in SST cooling. The R50 and R34 errors appear to have smaller slopes of 0.9 and 0.4°C per 100 km, respectively. Similar outcomes can be found in JTWCO set, although the wind radii errors are much smaller (Figure 11). This result is generally consistent with Pun et al. (2018), who made conclusions based on a single typhoon case. Of the three wind radii, R64 is clearly the most important for SST cooling estimates from 3DPWP.

But why is R64 so important for SST cooling? To investigate further, let's explore the TC's Integrated Kinetic Energy (IKE). Proposed by Powell and Reinhold (2007) and discussed in Knaff et al. (2013) with respect to ocean impacts, IKE is used to estimate TC energy available to transfer to the ocean. Since our focus is on TC winds, the IKE is modified so that it only represents the winds above gale force (i.e., 34 kt). Given the radial wind profile, IKE is computed via:

$$IKE = \int_A \frac{1}{2}\rho\left(U - 17.5\right)^2 hdA, \quad (1)$$

where ρ is air density taken as 1.15 kg m^3, U is wind speed in m s^{-1}, A is the total TC area defined by R34, h is the air vertical depth taken as 1 m. Basically, it is an integration of wind energy relative to the gale-forced wind over the TC area, as depicted by the outermost circle in Figure 1.

Using the radial wind profile of Super Typhoon Mangkhut at 1800 UTC September 12, 2018 as our test case, we compute IKE while varying individual wind radii ±35 km at a 5-km intervals (Figure 12), varying only one radius at a time. Figure 13 shows the change in IKE due to change in radii. IKE increases sharply as R64 is increased while rates of change are much lower for the R50 and R34 with R34 having the least impact. R64 is clearly most responsible for IKE in our idealized TCs, and hence has a stronger impact on SST cooling in our simulations.

4. Discussion

4.1. Model Dependence

Although the 3DPWP is thought to be one of the best ocean models to simulate ocean response to the TC (Balaguru et al., 2015; D'Asaro et al., 2014; Lin et al., 2013, 2021; Pun et al., 2018), and is consistent with satellite observations (cf. Figure 2b) in our data set, the results could be model dependent. To address this concern we use another well-regarded ocean model, the one-dimensional (1D) Mellor-Yamada ocean-mixed layer model (Mellor & Yamada, 1982) to run the same tests. The 1D Mellor-Yamada model has also been used to simulate the upper ocean mixing under TCs (Lin et al., 2008, 2009). As seen in Figure 14, the results from the 1D Mellor-Yamada model are consistent with those from the 3DPWP (cf. Figure 7), such that SST cooling error findings are likely model independent.

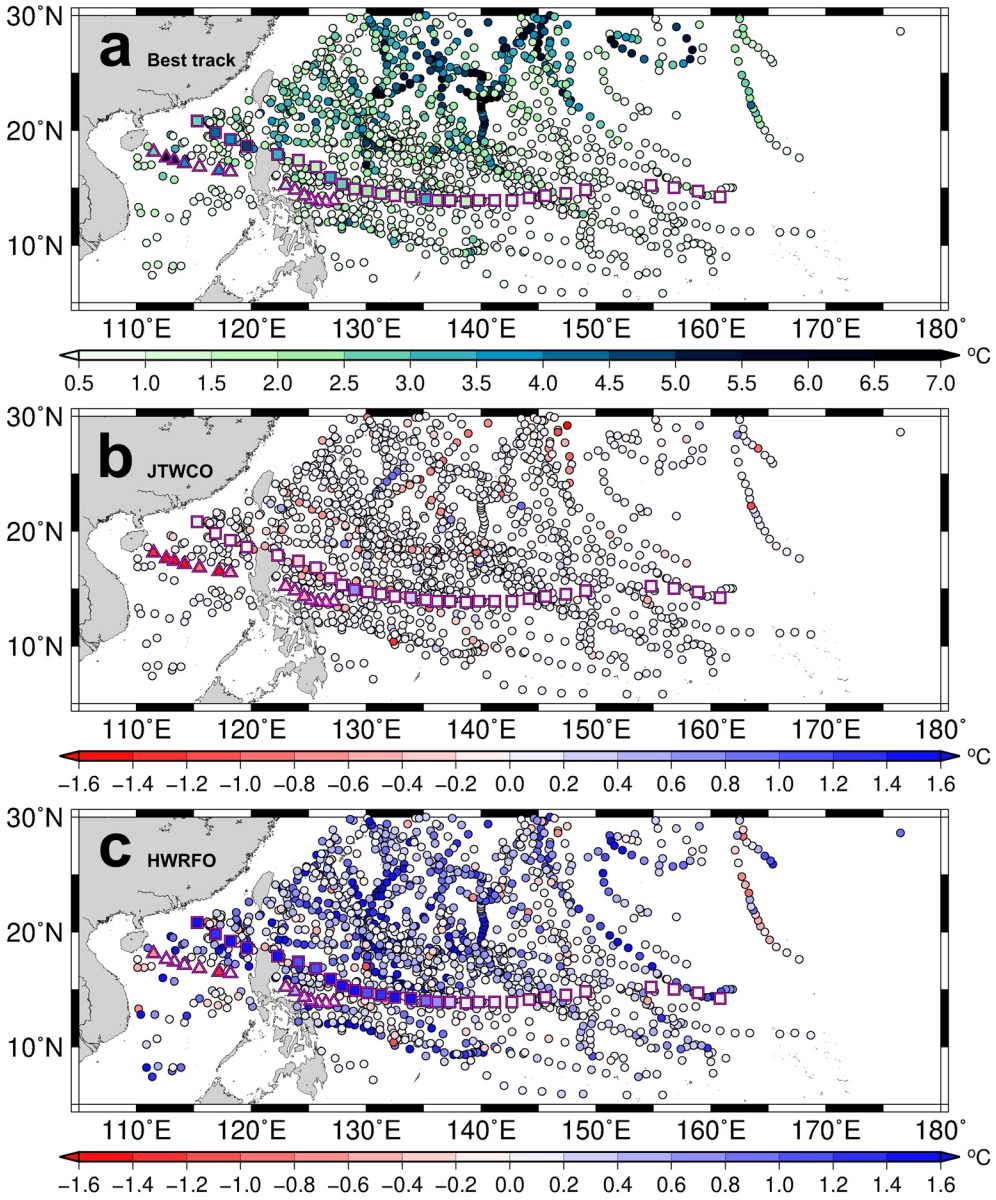

Figure 5. (a) Sea surface temperature (SST) cooling for 1,391 homogeneous tropical cyclone cases during 2014–2018, estimated by the three-dimensional Price-Weller-Pinkel Ocean Model that is initialized with the Joint Typhoon Warning Center (JTWC) best track data and Argo temperature profiles. (b) Differences in SST cooling as compared to (a) for using the analysis field (0 h) of the wind radii from JTWCO. (c) Same as (b), but for HWRFO. In (b) and (c), positive values indicate that the SST cooling is larger than that in (a). Squares indicate Typhoon Mangkhut (2018) and triangles indicate Typhoon Sarika (2016).

4.2. SST Cooling Errors Under TC

In this study, the SST cooling is nominally defined as the lowest SST point immediately after TC passage, which can be interpreted as the SST cooling in the TC outer core (cf. Figure 1b). But how applicable these results are to the TC inner core, where subtle changes in SST can have dramatic consequences on TC intensity change (Emanuel, 1999; Cione et al., 2013; Shay et al., 2000)? To evaluate this, we conducted another set of analysis using the maximum SST cooling within R64, which we used as a proxy for the TC inner core. Results show that, on average, the TC inner core SST cooling is systematically

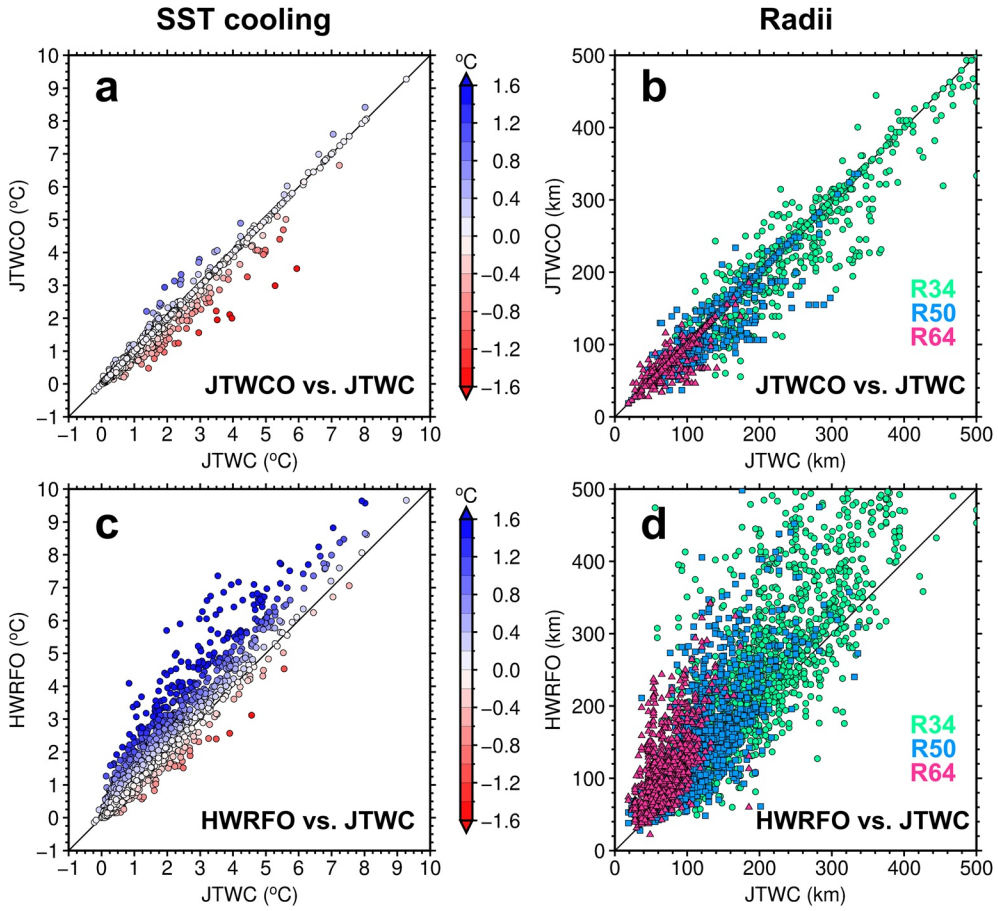

Figure 6. (a) Sea surface temperature cooling scatter plots for JTWCO versus Joint Typhoon Warning Center (JTWC) in 0 h experiments (i.e., analysis field). (b) Same as (a), but for wind radii. (c), (d) Same as (a), (b), but for HWRFO versus JTWC. The color code in (a), (c) indicates the cooling differences as compared to the baseline cooling (JTWC), and is for data in Figures 5b and 5c, respectively. In (b), (d) green circles, blue squares and magenta triangles indicate R34, R50, and R64, respectively.

smaller than the outer core cooling by about 0.3–0.6°C (not shown). This is expected because the outer core is exposed to wind forcing for longer duration, and that leads to enhanced vertical mixing and upwelling.

Figure 15 shows the mean SST cooling errors underneath the TC core (i.e., within R64) due to the uncertainty of wind radii. The results are consistent with those in Figure 7, and mean errors in Figure 15 are in fact similar to those in Figure 7. Interestingly, however, the error percentages tend to be larger associated with

Table 2
Five-Year Mean Baseline SST Cooling From Best Track and Mean Baseline Relative Cooling Based on Wind Radii From JTWCO and HWRFO

Time steps	0	12	24	36	48	72
Best track (cooling)	1.72 ± 1.54	1.94 ± 1.60	2.04 ± 1.59	2.11 ± 1.59	2.24 ± 1.62	2.38 ± 1.61
JTWCO (relative cooling)	−0.04 ± 0.23	−0.01 ± 0.41	0.00 ± 0.44	0.01 ± 0.47	0.02 ± 0.48	0.02 ± 0.5
HWRFO (relative cooling)	0.45 ± 0.65	0.42 ± 0.60	0.41 ± 0.61	0.41 ± 0.63	0.43 ± 0.65	0.48 ± 0.69
Sample size	1,391	1,103	1,025	977	877	733

Note. Cooling is in unit °C, with positive meaning larger than baseline. The standard deviations for the cooling are also shown.

Abbreviations: HWRFO, operational Hurricane Weather Research and Forecasting model; JTWCO, Joint Typhoon Warning Center official forecast; SST, sea surface temperature.

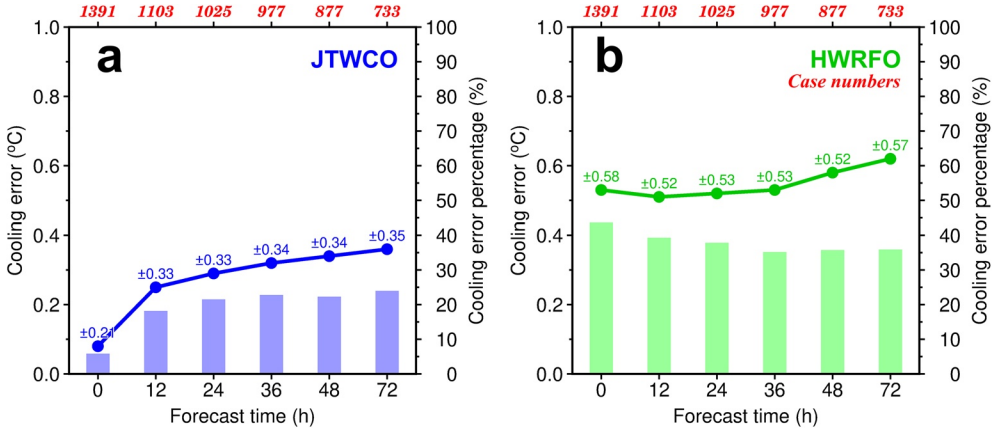

Figure 7. (a) Mean sea surface temperature (SST) cooling error induced by JTWCO's wind radii for the time steps of 0, 12, 24, 36, 48, and 72 h for the 2014–2018 homogeneous data set. (b) Same as (a), but for HWRFO's wind radii. Curves represent the mean absolute errors with the numbers showing the standard deviations, while bars represent mean error percentages with respect to SST cooling estimated from the best track. The number of cases are shown in red.

the inner core SST cooling. On average, the errors increase by 5% for JTWCO and 11% for HWRFO for the inner core SST cooling. Similar results are found for the maximum SST cooling for the R34 and R50 experiments. From these results we can further confirm that uncertainty in the wind radii forecasts could alter the entire SST cooling structure under and within the TC, which in turn affects TC intensity.

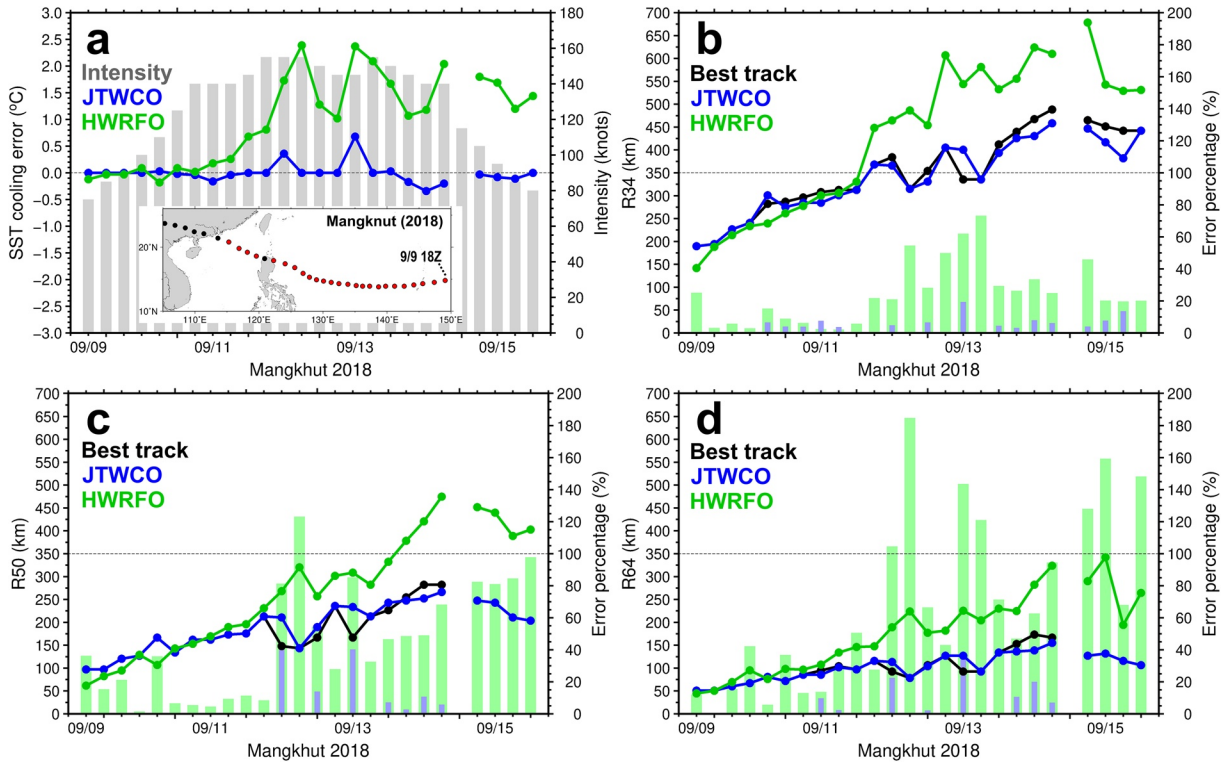

Figure 8. (a) Six-hourly along-track sea surface temperature (SST) cooling errors induced by JTWCO and HWRFO's wind radii analysis (0 h) for Super Typhoon Mangkhut (2018). Gray bars represent 1-min sustained surface winds in knots. (b)–(d) Inter-comparisons of wind radii among three sources for R34, R50, and R64, respectively. Vertical bars indicated the error percentages with respect to the best track. Horizontal dashed lines depict the levels of zero SST cooling error in (a) and 100% error in (b)–(d). The color legend is shown at the upper-left corner of each plot. The track of Mangkhut is shown in (a) and also can be found in Figure 5. Red dots in subfigure of (a) indicate the cases that are simulated by the three-dimensional Price-Weller-Pinkel Ocean Model.

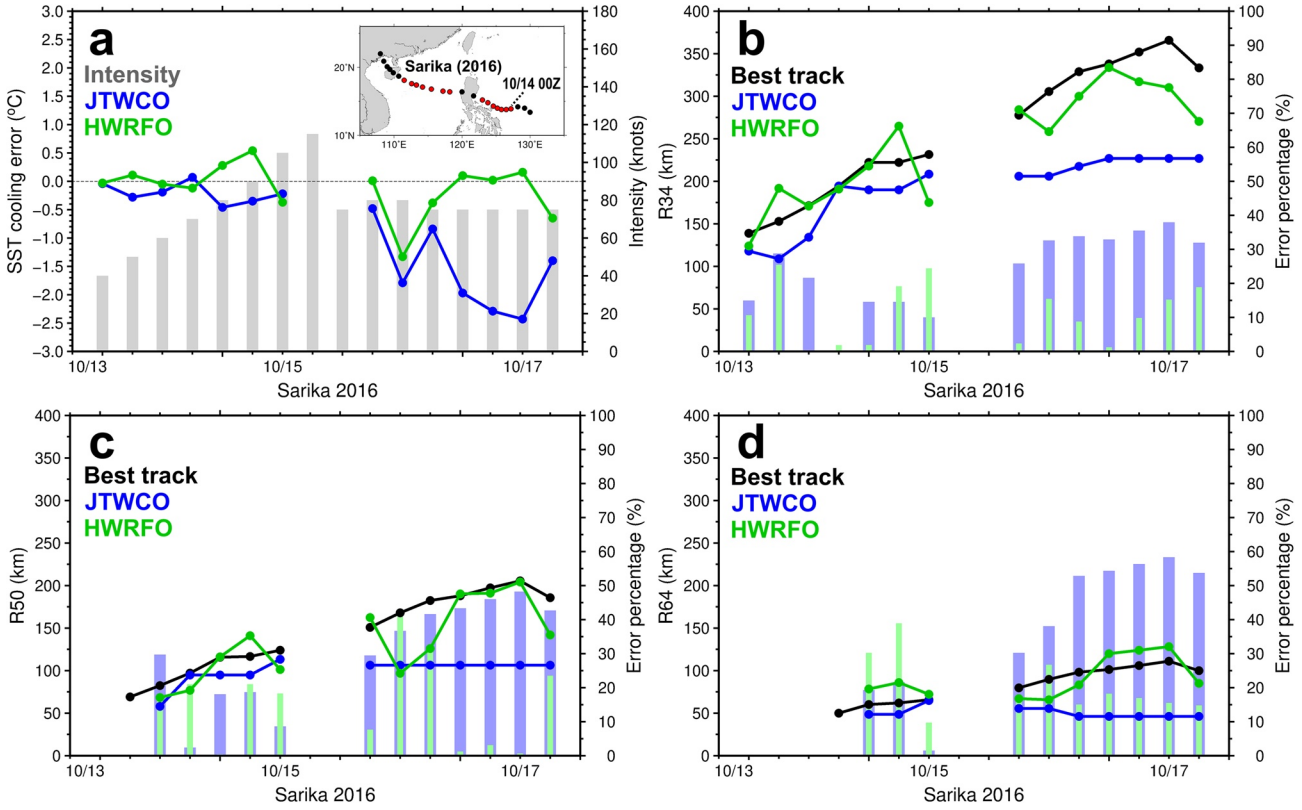

Figure 9. Same as Figure 8, but for Typhoon Sarika (2016).

4.3. The Importance of Wind Radii on SST Cooling

SST cooling is an important controlling factor in TC intensity and size changes. The intensification process is complex, involving multiple spatial and temporal scales with interactions between the TC, the ocean below, and the surrounding atmosphere. One important aspect of TC intensification is the energy fluxed from the ocean. This flux is largely determined by air-sea temperature and moisture differences and requires accurate TC induced SST cooling estimates. Most efforts to investigate SST cooling associated with TCs have focused on the role of ocean thermal structure, TC translation speed and maximum surface winds (intensity). TC size or more specifically the radial structure of surface wind, has been mostly overlooked in TC-ocean research. Yet, from our 3DPWP simulations, it is apparent that TC size (defined as R34, R50, and

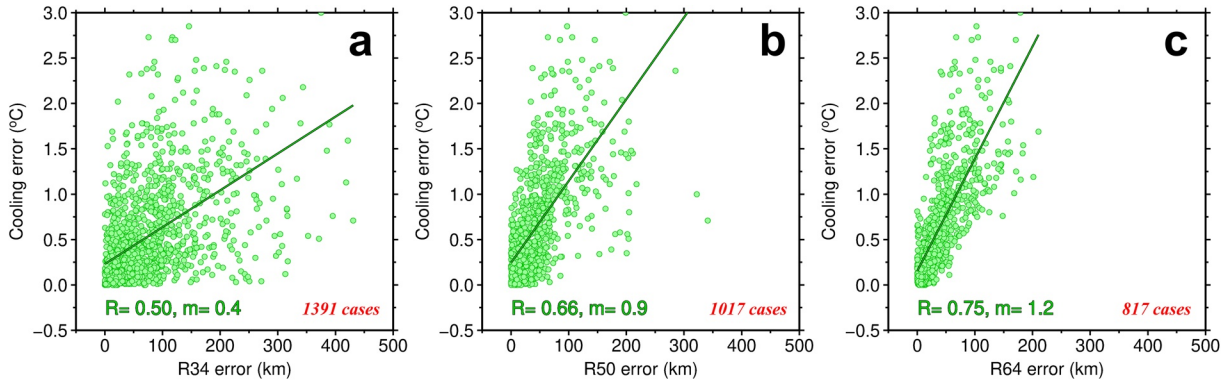

Figure 10. Absolute sea surface temperature cooling error versus absolute error in (a) R34, (b) R50, and (c) R64 for the analysis field of HWRFO over the years from 2014 to 2018. Correlation coefficients (R), linear regression lines and case numbers are shown. The slope (m) is with the unit °C/100 km. All the correlations are statistically significant at 99% in student-t tests.

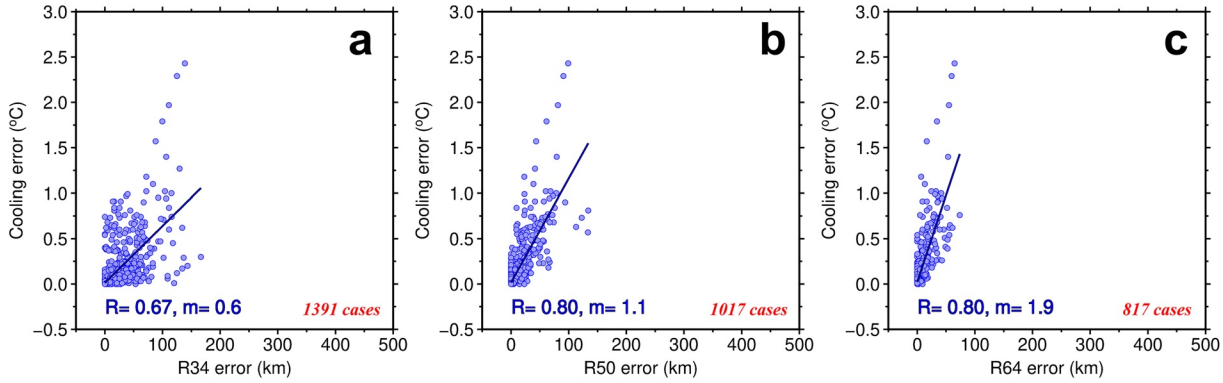

Figure 11. Same as Figure 10, but for JTWCO. All the correlations are statistically significant at 99% in student-t tests.

R64) is well-correlated with SST cooling (Figures 10 and 11). This correlation is higher than other factors, that is, TC translation speed, maximum wind, and upper ocean heat content, and suggests that it is at least as important as those factors (Figure 16).

From Figures 10 and 11 and the IKE analysis (Figure 13), we found that SST cooling is most sensitive to R64. This is somewhat troubling as these inner core winds are the most difficult to measure and least frequently observed. At JTWC the problem has been so acute that until recently the R50 and R64 in best tracks have been assigned through empirical relationships using R34 (Knaff & Sampson, 2015; Sampson & Knaff, 2015; Sampson et al., 2017, 2018). Storm-penetrating aircraft observations (e.g., Black et al., 2007) are scarce especially in the western North Pacific (D'Asaro et al., 2014; Wu et al., 2005).

There is hope though. New inner core remotely sensed observations that use cross-polarization, such as those from Synthetic Aperture Radar (SAR), can instantaneously estimate the surface winds (see Combot et al., 2020; Mouche et al., 2019) and are becoming available to operations in near real-time. To augment SAR observations, other all-weather wind estimates from multi-banded (Alsweiss et al., 2018; Chang et al., 2015; Shibata, 2002, 2006) and L band radiometers (Meissner et al., 2017; Reul et al., 2016, 2017; Yueh et al., 2016) also help, but are often limited by their >20 km resolutions and/or latency issues. Until high resolutions and inner core wind speeds become routinely available, R34, R50, and R64 forecasts from JTWC and other operational centers will remain useful for models like 3DPWP. Although sophisticated dynamical models can currently estimate winds gross features of the inner core, prediction of SST cooling requires that these models also accurately forecast inner core surface winds at very high resolution (Bender et al., 2017, 2019; Chen et al., 2019; Dong et al., 2020; Tallapragada et al., 2014), which is still a challenge.

4.4. The Impact on TC Intensity Forecasting

Using one of state-of-the-art hurricane models from the Geophysical Fluid Dynamics Laboratory, Bender et al. (2017) pointed out that the storm size may be critical to the success of TC intensity prediction and that proper specification of the gale force wind radii and the storm size may be critical to achieving a more reliable forecast of RI using high-resolution regional models. Bender et al. (2017) did not examine differences in the ocean cooling in the different initializations, but their paper furthers our contention that TC surface wind structure is important for modeling TC intensity. Given the evidence from this study, SST cooling is indeed positively proportional to the size of the TC, but how exactly the TC responds to the cooling underneath is still not fully understood. For instance, Lee and Chen (2014) proposed that SST cooling might have a positive role in TC intensification through stabilization of the boundary layer in the outer core. Others factors include the efficiency of TC energy transfer, which is related to the entire three dimensional structure of the TC (Emanuel, 1986; Emanuel et al., 2004). In the future, in-depth and systematic investigations with coupled models may provide a further clarification on the interactions of TC size, SST cooling, and TC intensity.

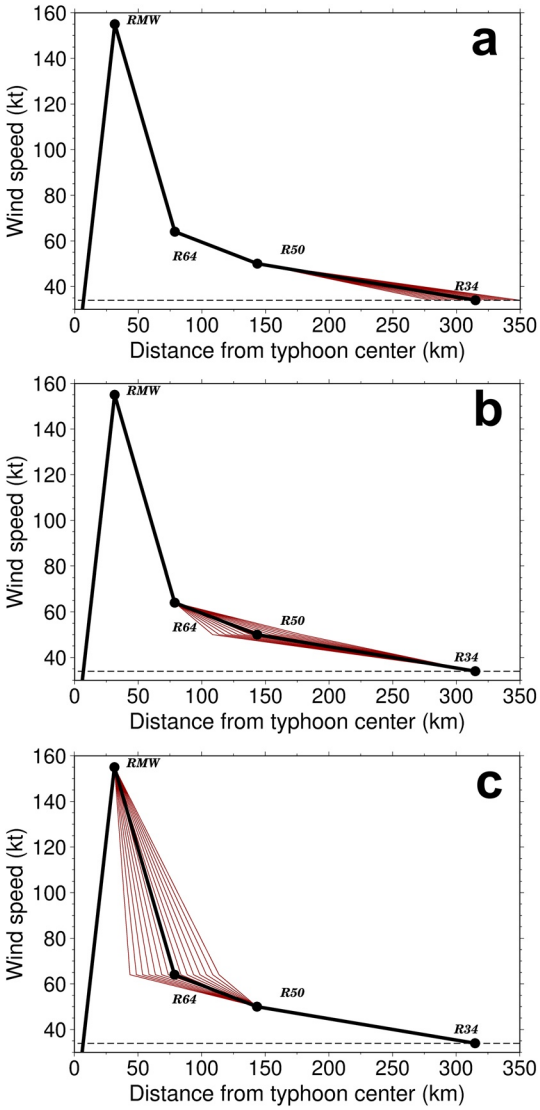

Figure 12. Illustration of (a) 34 kt, (b) 50 kt, and (c) 64 kt radial wind profiles used in sensitivity tests. The wind profile is based on the best track data of Super Typhoon Mangkhut at 1800 UTC 12 September 2018. Each wind radius (i.e., R34, R50, and R64) is perturbed from −35 to 35 km at 5 km intervals from the best track values, as depicted by red lines. The horizontal dashed line indicates 34 kt wind.

5. Conclusions

This study systematically analyzed the operational wind radii forecasts from JTWC and the HWRF model for the period of 2014–2018 in the western North Pacific. This is accomplished by using the JTWC best tracks as the control group, and replacing only the R34, R50, and R64 with those from either the JTWC (JTWCO) or HWRF model (HWRFO) forecasts. Results show large differences between these two data sets (Figures 3 and 4). The JTWCO wind radii uncertainty in terms of error percentage increases from R34 to R64. The errors are small (∼5% error) at analysis time, then grow dramatically to 12 h with slower increases out to 72 h. Furthermore, there is no obvious bias in JTWCO's wind radii. For HWRFO, the highest wind radii uncertainty usually occurs in the analysis field, but the error tends to decrease within the first 24 h. Thereafter forecast wind radii uncertainty increases gradually with forecast time. HWRFO's analysis and forecasts have large positive biases, indicating that it tends to overestimate TC wind radii for this study period.

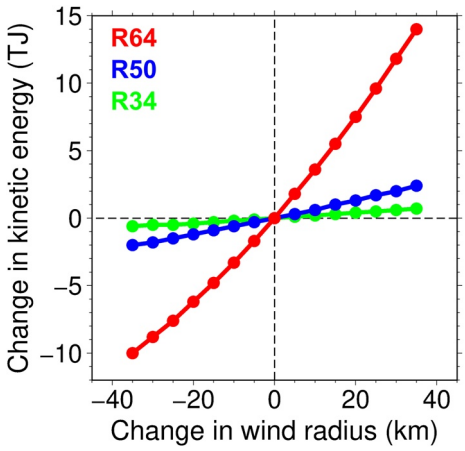

Figure 13. Changes in Integrated Kinetic Energy versus changes in radii for cases shown in Figure 12. Each dot corresponds to one radial wind profile in Figure 12.

Based on a large number of 3DPWP ocean model simulations (15,983), potential errors in SST cooling due to wind radii uncertainty are quantified. The 5-year mean errors in simulated SST cooling with JTWCO analysis wind radii are ~6% of the baseline cooling using best tracks in 3DPWP, and rise to ~20% in the forecasts (Figure 7a). With HWRFO as input to 3DPWP, the percentage errors start at ~40% of the SST cooling, then drop to ~35% (Figure 7b). The wind radii do indeed have a significant effect on SST cooling estimation—1D Mellor-Yamada model-based results are similar (Figure 14). These results carry over to the inner core cooling errors occurring underneath the evolving TC (i.e., within R64) with similar mean error values, but with larger error percentages (Figure 15). JTWC operational data tends to provide better results if we assume that the best track is ground truth. Analysis of two recent typhoons (Mangkhut and Sarika) suggests that variations in wind radii uncertainty can be large in these two operational data sets. Such TC size uncertainty leads to substantial SST cooling errors in the range ±2.4°C. Such large errors can be critical for TC intensity predictions, especially when the TC is about to make landfall. In conclusion, the R34, R50, and R64 analyses and forecasts, proxies for TC structure, are critical parameters for ocean SST prediction both during and following TC passage. They must be considered along with other forecast parameters (i.e., translation speed, V_{max}, and upper ocean heat content) in order to yield more realistic ocean response. With a better understanding of the role of wind radii and their associated uncertainties, predictions and simulations of TC intensity change could be further improved in the future.

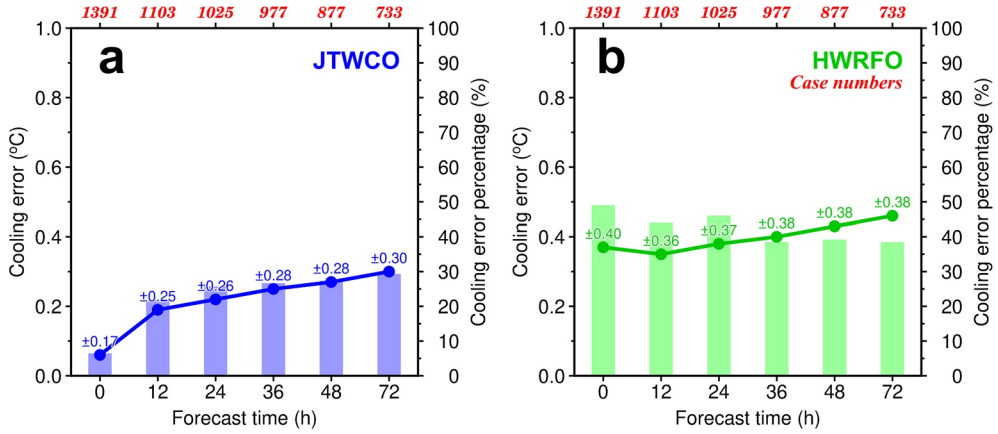

Figure 14. Cooling error plots as in Figure 7, but based on the one-dimensional Mellor-Yamada Model.

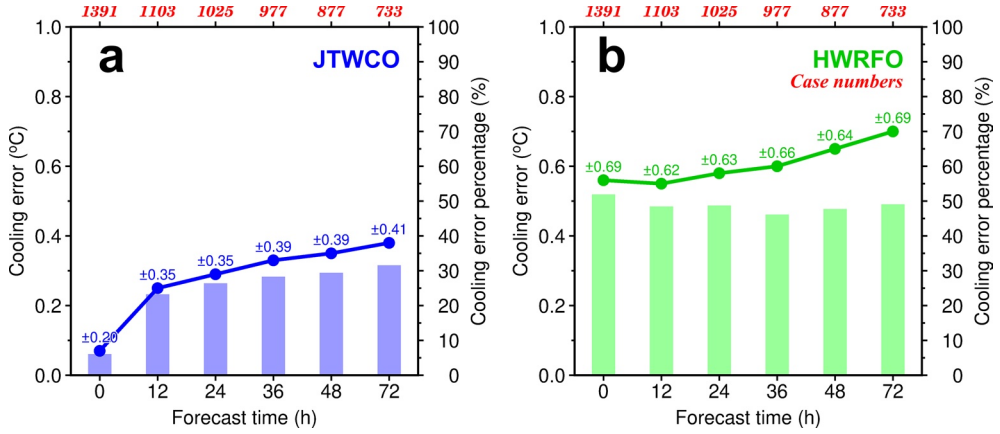

Figure 15. Cooling error plots as in Figure 7, but based on the maximum sea surface temperature cooling within R64.

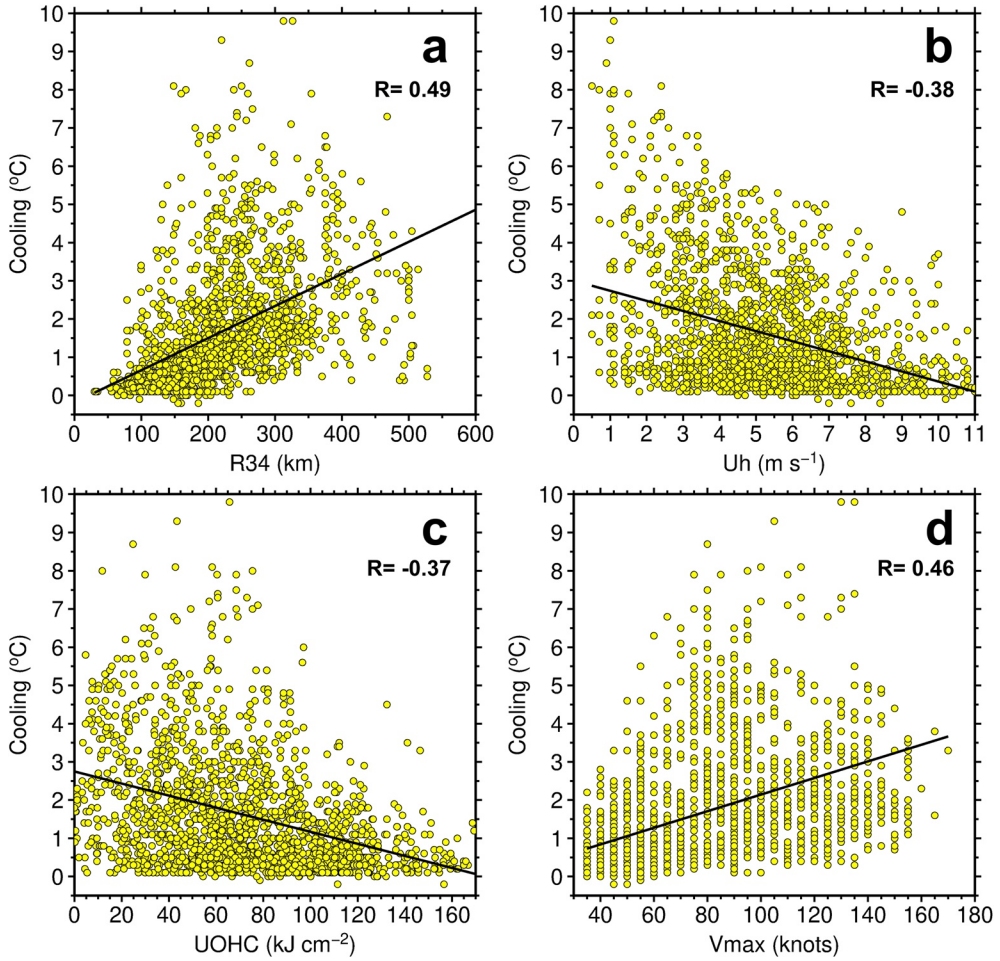

Figure 16. Sea surface temperature cooling versus (a) R34, (b) translation speed (Uh), (c) upper ocean heat content, and (d) V_{max}. Results are derived from the SST cooling simulations (1,765 cases) for the Joint Typhoon Warning Center best track and Argo temperature profiles (i.e., control group). The correlation coefficients and linear regression lines are shown. All the correlations are statistically significant at 99% through the student-t tests.

Data Availability Statement

Operational TC wind radii analyses and forecasts are archived on the JTWC collaboration site (https://pzal.metoc.navy.mil). TC best tracks are available at JTWC's best track archive (https://www.metoc.navy.mil/jtwc/jtwc.html). Monthly gridded Argo data are distributed on Roemmich-Gilson Argo Climatology website of Scripps Institution of Oceanography (http://sio-argo.ucsd.edu/RG_Climatology.html). OISST data are provided by Remote Sensing Systems (http://www.remss.com/).

Acknowledgments
The authors thank JTWC for the best track and operational typhoon data sets, Scripps Institution of Oceanography for the monthly gridded Argo data, Remote Sensing Systems for the IOSST product, and Dr. James F. Price of Woods Hole Oceanographic Institution for the 3DPWP ocean model. Thanks also to the three anonymous reviewers, their insightful comments helped improve the quality of this work. I.-F. Pun is supported by Grant MOST 107-2111-M-008-001-MY3, MOST 109-2111-M-008-011 and MOST 110-2111-M-008-015. J. Knaff thanks NOAA/NESDIS for providing base funding for his efforts. C. R. Sampson is supported by funding from the Office of Naval Research, Program Elements 0602435N and 0603207N. The authors acknowledge support from the Office of Naval Research for supporting NRL tropical cyclone research. The views, opinions, and findings contained in this report are those of the authors and should not be construed as an official National Oceanic and Atmospheric Administration or U.S. Government position, policy, or decision.

References

Alsweiss, S., Sapp, J., Jelenak, Z., & Chang, P. (2018). Validation of AMSR2 oceanic environmental data records using tropical cyclone composite fields. In *IGARSS 2018 - 2018 IEEE International Geoscience and Remote Sensing Symposium, Valencia, 2018* (pp. 3078–3081). https://doi.org/10.1109/IGARSS.2018.8517426

Argo Science Team. (2000). *Report of the Argo Science Team 2nd Meeting (AST-2) March 7-9, 2000*. Southampton Oceanography Centre.

Balaguru, K., Foltz, G. R., Leung, L. R., D'Asaro, E., Emanuel, K. A., Liu, H. L., & Zedler, S. E. (2015). Dynamic Potential Intensity: An improved representation of the ocean's impact on tropical cyclones. *Geophysical Research Letters*, *42*(16), 6739–6746. https://doi.org/10.1002/2015gl064822

Balaguru, K., Foltz, G. R., Leung, L. R., Kaplan, J., Xu, W., Reul, N., & Chapron, B. (2020). Pronounced impact of salinity on rapidly intensifying tropical cyclones. *Bulletin of the American Meteorological Society*, *101*(9), E1497–E1511. https://doi.org/10.1175/bams-d-19-0303.1

Bender, M. A., Marchok, T., Tuleya, R. E., Ginis, I., Tallapragada, V., & Lord, S. J. (2019). Hurricane Model Development at GFDL: A collaborative success story from a historical perspective. *Bulletin of the American Meteorological Society*, *100*(9), 1725–1736. https://doi.org/10.1175/bams-d-18-0197.1

Bender, M. A., Marchok, T. P., Sampson, C. R., Knaff, J. A., & Morin, M. J. (2017). Impact of storm size on prediction of storm track and intensity using the 2016 operational GFDL Hurricane Model. *Weather and Forecasting*, *32*(4), 1491–1508. https://doi.org/10.1175/waf-d-16-0220.1

Black, P. G., D'Asaro, E. A., Drennan, W. M., French, J. R., Niiler, P. P., Sanford, T. B., et al. (2007). Air-sea exchange in hurricanes – synthesis of observations from the coupled boundary layer air-sea transfer experiment. *Bulletin of the American Meteorological Society*, *88*(3), 357–374. https://doi.org/10.1175/bams-88-3-357

Cangialosi, J. P., Blake, E., DeMaria, M., Penny, A., Latto, A., Rappaport, E., & Tallapragada, V. (2020). Recent progress in tropical cyclone intensity forecasting at the National Hurricane Center. *Weather and Forecasting*, *35*, 1913–1922. https://doi.org/10.1175/WAF-D-20-0059.1

Chan, K. T. F., & Chan, J. C. L. (2012). Size and strength of tropical cyclones as inferred from QuikSCAT data. *Monthly Weather Review*, *140*(3), 811–824. https://doi.org/10.1175/mwr-d-10-05062.1

Chan, K. T. F., & Chan, J. C. L. (2013). Angular momentum transports and synoptic flow patterns associated with tropical cyclone size change. *Monthly Weather Review*, *141*(11), 3985–4007. https://doi.org/10.1175/mwr-d-12-00204.1

Chan, K. T. F., & Chan, J. C. L. (2015). Global climatology of tropical cyclone size as inferred from QuikSCAT data. *International Journal of Climatology*, *35*(15), 4843–4848. https://doi.org/10.1002/joc.4307

Chang, P., Z. Jelenak, S. Alsweiss, & Sapp, J. (2015). *Algorithm theoretical basis document: GCOM-W1/AMSR2 Day-2 EDR, version 2* (p. 22). Retrieved from https://www.star.nesdis.noaa.gov/jpss/documents/ATBD/ATBD_AMSR2_Ocean_EDR_v2.0.pdf

Chang, Y. T., Lin, I. I., Huang, H. C., Liao, Y. C., & Lien, C. C. (2020). The association of typhoon intensity increase with translation speed increase in the South China Sea. *Sustainability-Basel*, *12*(3). https://doi.org/10.3390/su12030939

Chen, J.-H., Lin, S.-J., Zhou, L., Chen, X., Rees, S., Bender, M., & Morin, M. (2019). Evaluation of tropical cyclone forecasts in the next generation global prediction system. *Monthly Weather Review*, *147*(9), 3409–3428. https://doi.org/10.1175/mwr-d-18-0227.1

Chen, S. Y. S., Price, J. F., Zhao, W., Donelan, M. A., & Walsh, E. J. (2007). The CBLAST-hurricane program and the next-generation fully coupled atmosphere-wave-ocean. Models for hurricane research and prediction. *Bulletin of the American Meteorological Society*, *88*(3), 311–318. https://doi.org/10.1175/bams-88-3-311

Chu, J. H., Sampson, C., Levine, A. S. & Fukada, E. (2002). *The joint typhoon warning center tropical cyclone best-tracks, 1945–2000*. Joint Typhoon Warning Center.

Cione, J. J., Kalina, E. A., Zhang, J. A., & Uhlhorn, E. W. (2013). Observations of air-sea interaction and intensity change in hurricanes. *Monthly Weather Review*, *141*(7), 2368–2382. https://doi.org/10.1175/mwr-d-12-00070.1

Cione, J. J., & Uhlhorn, E. W. (2003). Sea surface temperature variability in hurricanes: Implications with respect to intensity change. *Monthly Weather Review*, *131*(8), 1783–1796. https://doi.org/10.1175//2562.1

Combot, C., Mouche, A., Knaff, J., Zhao, Y., Zhao, Y., Vinour, L., et al. (2020). Extensive High-Resolution Synthetic Aperture Radar (SAR) data analysis of tropical cyclones: Comparisons with SFMR flights and best track. *Monthly Weather Review*, *148*(11), 4545–4563. https://doi.org/10.1175/mwr-d-20-0005.1

D'Asaro, E. A., Black, P. G., Centurioni, L. R., Chang, Y. T., Chen, S. S., Foster, R. C., et al. (2014). Impact of typhoons on the ocean in the Pacific. *Bulletin of the American Meteorological Society*, *95*(9), 1405–1418.

DeMaria, M., Knaff, J. A., Brennan, M. J., Brown, D., Knabb, R. D., DeMaria, R. T., et al. (2013). Improvements to the Operational Tropical Cyclone Wind Speed Probability Model. *Weather and Forecasting*, *28*(3), 586–602. https://doi.org/10.1175/waf-d-12-00116.1

DeMaria, M., Sampson, C. R., Knaff, J. A., & Musgrave, K. D. (2014). Is tropical cyclone intensity guidance improving? *Bulletin of the American Meteorological Society*, *95*(3), 387–398. https://doi.org/10.1175/bams-d-12-00240.1

Dong, J., Liu, B., Zhang, Z., Wang, W., Mehra, A., Hazelton, A. T., et al. (2020). The Evaluation of Real-Time Hurricane Analysis and Forecast System (HAFS) Stand-Alone Regional (SAR) Model Performance for the 2019 Atlantic Hurricane Season. *Atmosphere*, *11*(6), 617. https://doi.org/10.3390/atmos11060617

Emanuel, K. A. (1986). An air-sea interaction theory for tropical cyclones. Part I: Steady-state maintenance. *Journal of the Atmospheric Sciences*, *43*(6), 585–605. https://doi.org/10.1175/1520-0469(1986)043<0585:aasitf>2.0.co;2

Emanuel, K. A. (1999). Thermodynamic control of hurricane intensity. *Nature*, *401*(6754), 665–669. https://doi.org/10.1038/44326

Emanuel, K. A. (2020). Evidence that hurricanes are getting stronger. *Proceedings of the National Academy of Sciences*, *117*(24), 13194–13195. https://doi.org/10.1073/pnas.2007742117

Emanuel, K. A., DesAutels, C., Holloway, C., & Korty, R. (2004). Environmental control of tropical cyclone intensity. *Journal of the Atmospheric Sciences*, *61*(7), 843–858. https://doi.org/10.1175/1520-0469(2004)061<0843:ecotci>2.0.co;2

Ford, V. L., Walker, N. D., & Pun, I. F. (2020). Anomalous oceanic conditions in the Central and Eastern North Pacific Ocean during the 2014 Hurricane season and relationships to three major hurricanes. *Journal of Marine Science and Engineering*, *8*(4). https://doi.org/10.3390/jmse8040288

Gentemann, C. L., Donlon, C. J., Stuart-Menteth, A., & Wentz, F. J. (2003). Diurnal signals in satellite sea surface temperature measurements. *Geophysical Research Letters*, *30*(3), 1140. https://doi.org/10.1029/2002GL016291

Glenn, S. M., Miles, T. N., Serokal, G. N., Xu, Y., Forney, R. K., Yu, F., et al. (2016). Stratified coastal ocean interactions with tropical cyclones. *Nature Communications*, *7*. https://doi.org/10.1038/ncomms10887

Guan, S. D., Zhao, W., Huthnance, J., Tian, J. W., & Wang, J. H. (2014). Observed upper ocean response to typhoon Megi (2010) in the Northern South China Sea. *Journal of Geophysical Research: Oceans*, *119*(5), 3134–3157. https://doi.org/10.1002/2013jc009661

Hill, K. A., & Lackmann, G. M. (2009). Influence of environmental humidity on tropical cyclone size. *Monthly Weather Review*, *137*(10), 3294–3315. https://doi.org/10.1175/2009mwr2679.1

Holland, G. J., Belanger, J. I., & Fritz, A. (2010). A revised model for radial profiles of hurricane winds. *Monthly Weather Review*, *138*(12), 4393–4401. https://doi.org/10.1175/2010mwr3317.1

Hong, X. D., Chang, S. W., Raman, S., Shay, L. K., & Hodur, R. (2000). The interaction between Hurricane Opal (1995) and a warm core ring in the Gulf of Mexico. *Monthly Weather Review*, *128*(5), 1347–1365. https://doi.org/10.1175/1520-0493(2000)128<1347:tibhoa>2.0.co;2

Huang, P., Lin, I. I., Chou, C., & Huang, R. H. (2015). Change in ocean subsurface environment to suppress tropical cyclone intensification under global warming. *Nature Communications*, *6*. https://doi.org/10.1038/ncomms8188

Jaimes, B., Shay, L. K., & Uhlhorn, E. W. (2015). Enthalpy and momentum fluxes during hurricane earl relative to underlying ocean features. *Monthly Weather Review*, *143*(1), 111–131. https://doi.org/10.1175/mwr-d-13-00277.1

Kaplan, J., Rozoff, C. M., DeMaria, M., Sampson, C. R., Kossin, J. P., Velden, C. S., et al. (2015). Evaluating environmental impacts on tropical cyclone rapid intensification predictability utilizing statistical models. *Weather and Forecasting*, *30*(5), 1374–1396. https://doi.org/10.1175/WAF-D-15-0032.1

Knaff, J. A., DeMaria, M., Sampson, C. R., Peak, J. E., Cummings, J., & Schubert, W. H. (2013). Upper oceanic energy response to tropical cyclone passage. *Journal of Climate*, *26*(8), 2631–2650. https://doi.org/10.1175/jcli-d-12-00038.1

Knaff, J. A., & Sampson, C. R. (2015). After a decade are Atlantic Tropical Cyclone Gale force wind radii forecasts now skillful? *Weather and Forecasting*, *30*(3), 702–709. https://doi.org/10.1175/waf-d-14-00149.1

Ko, D. S., Chao, S. Y., Wu, C. C., & Lin, I. I. (2014). Impacts of Typhoon Megi (2010) on the South China Sea. *Journal of Geophysical Research: Oceans*, *119*(7), 4474–4489. https://doi.org/10.1002/2013jc009785

Landsea, C. W., & Franklin, J. L. (2013). Atlantic Hurricane Database uncertainty and presentation of a new database format. *Monthly Weather Review*, *141*(10), 3576–3592. https://doi.org/10.1175/mwr-d-12-00254.1

Lee, C. Y., & Chen, S. Y. S. (2014). Stable boundary layer and its impact on tropical cyclone structure in a coupled atmosphere-ocean model. *Monthly Weather Review*, *142*(5), 1927–1944. https://doi.org/10.1175/mwr-d-13-00122.1

Lin, I. I., Black, P., Price, J. F., Yang, C. Y., Chen, S. S., Lien, C. C., et al. (2013). An ocean coupling potential intensity index for tropical cyclones. *Geophysical Research Letters*, *40*(9), 1878–1882. https://doi.org/10.1002/grl.50091

Lin, I. I., Pun, I. F., & Lien, C. C. (2014). "Category-6" supertyphoon Haiyan in global warming hiatus: Contribution from subsurface ocean warming. *Geophysical Research Letters*, *41*(23), 8547–8553. https://doi.org/10.1002/2014gl061281

Lin, I. I., Pun, I. F., & Wu, C. C. (2009). Upper-ocean thermal structure and the Western North Pacific category 5 typhoons. Part II: Dependence on translation speed. *Monthly Weather Review*, *137*(11), 3744–3757. https://doi.org/10.1175/2009mwr2713.1

Lin, I.-I., Rogers, R. F., Huang, H.-C., Liao, Y.-C., Herndon, D., Yu, J.-Y., et al. (2021). A tale of two rapidly-intensifying supertyphoons: Hagibis (2019) and Haiyan (2013). *Bulletin of the American Meteorological Society*, 1–59. https://doi.org/10.1175/bams-d-20-0223.1

Lin, I. I., Wu, C. C., Emanuel, K. A., Lee, I. H., Wu, C. R., & Pun, I. F. (2005). The interaction of Supertyphoon Maemi (2003) with a warm ocean eddy. *Monthly Weather Review*, *133*(9), 2635–2649. https://doi.org/10.1175/mwr3005.1

Lin, I. I., Wu, C. C., Pun, I. F., & Ko, D. S. (2008). Upper-ocean thermal structure and the western North Pacific category 5 typhoons. Part I: Ocean features and the category 5 typhoons' intensification. *Monthly Weather Review*, *136*(9), 3288–3306. https://doi.org/10.1175/2008mwr2277.1

Mei, W., Pasquero, C., & Primeau, F. (2012). The effect of translation speed upon the intensity of tropical cyclones over the tropical ocean. *Geophysical Research Letters*, *39*. https://doi.org/10.1029/2011gl050765

Mei, W., Xie, S. P., Primeau, F., McWilliams, J. C., & Pasquero, C. (2015). Northwestern Pacific typhoon intensity controlled by changes in ocean temperatures. *Science Advances*, *1*(4). https://doi.org/10.1126/sciadv.1500014

Meissner, T., Ricciardulli, L., & Wentz, F. J. (2017). Capability of the SMAP mission to measure ocean surface winds in storms. *Bulletin of the American Meteorological Society*, *98*(8), 1660–1677. https://doi.org/10.1175/BAMS-D-16-0052.1

Mellor, G. L., & Yamada, T. (1982). Development of a turbulence closure model for geophysical fluid problems. *Reviews of Geophysics*, *20*(4), 851–875. https://doi.org/10.1029/RG020i004p00851

Mok, D. K. H., Chan, J. C. L., & Chan, K. T. F. (2018). A 31-year climatology of tropical cyclone size from the NCEP Climate Forecast System Reanalysis. *International Journal of Climatology*, *38*, E796–E806. https://doi.org/10.1002/joc.5407

Mouche, A., Chapron, B., Knaff, J., Zhao, Y. L., Zhang, B., & Combot, C. (2019). Copolarized and cross-polarized SAR measurements for high-resolution description of major hurricane wind structures: Application to IRMA category 5 hurricane. *Journal of Geophysical Research: Oceans*, *124*(6), 3905–3922. https://doi.org/10.1029/2019jc015056

Peduzzi, P., Chatenoux, B., Dao, H., De Bono, A., Herold, C., Kossin, J., et al. (2012). Global trends in tropical cyclone risk. *Nature Climate Change*, *2*(4), 289–294. https://doi.org/10.1038/nclimate1410

Potter, H., DiMareo, S. F., & Knap, A. H. (2019). Tropical cyclone heat potential and the rapid intensification of Hurricane Harvey in the Texas Bight. *Journal of Geophysical Research: Oceans*, *124*(4), 2440–2451. https://doi.org/10.1029/2018jc014776

Powell, M. D., & Reinhold, T. A. (2007). Tropical cyclone destructive potential by integrated kinetic energy. *Bulletin of the American Meteorological Society*, *88*, 513–526. https://doi.org/10.1175/BAMS-88-4-513

Price, J. F. (1981). Upper ocean response to a hurricane. *Journal of Physical Oceanography*, *11*(2), 153–175. https://doi.org/10.1175/1520-0485(1981)011<0153:uortah>2.0.co;2

Price, J. F. (1983). Internal wave wake of a moving storm. Part I. Scales, energy budget and observations. *Journal of Physical Oceanography*, *13*(6), 949–965. https://doi.org/10.1175/1520-0485(1983)013<0949:iwwoam>2.0.co;2

Price, J. F., Sanford, T. B., & Forristall, G. Z. (1994). Forced stage response to a moving hurricane. *Journal of Physical Oceanography*, *24*(2), 233–260. https://doi.org/10.1175/1520-0485(1994)024<0233:fsrtam>2.0.co;2

Pun, I. F., Chan, J. C. L., Lin, I. I., Chan, K. T. E., Price, J. E., Ko, D. S., et al. (2019). Rapid intensification of typhoon Hato (2017) over shallow water. *Sustainability-Basel*, *11*(13). https://doi.org/10.3390/su11133709

Pun, I. F., Lin, I. I., Lien, C. C., & Wu, C. C. (2018). Influence of the size of supertyphoon Megi (2010) on SST cooling. *Monthly Weather Review*, *146*(3), 661–677. https://doi.org/10.1175/mwr-d-17-0044.1

Rappaport, E. N., Jiing, J. G., Landsea, C. W., Murillo, S. T., & Franklin, J. L. (2012). The joint hurricane test bed its first decade of tropical cyclone research-to-operations activities reviewed. *Bulletin of the American Meteorological Society*, *93*(3), 371–380. https://doi.org/10.1175/bams-d-11-00037.1

Reul, N., Chapron, B., Zabolotskikh, E., Donlon, C., Mouche, A., Tenerelli, J., et al. (2017). A new generation of tropical cyclone size measurements from space. *Bulletin of the American Meteorological Society*, *98*(11), 2367–2385. https://doi.org/10.1175/BAMS-D-15-00291.1

Reul, N., Chapron, B., Zabolotskikh, E., Donlon, C., Quilfen, Y., Guimbard, S., & Piolle, J. F. (2016). A revised L-band radio-brightness sensitivity to extreme winds under tropical cyclones: The five year SMOS-storm database. *Remote Sensing of Environment*, *180*, 274–291. https://doi.org/10.1016/j.rse.2016.03.011

Roemmich, D., & Gilson, J. (2009). The 2004-2008 mean and annual cycle of temperature, salinity, and steric height in the global ocean from the Argo Program. *Progress in Oceanography*, *82*(2), 81–100. https://doi.org/10.1016/j.pocean.2009.03.004

Rogers, R. F., Aberson, S., Bell, M. M., Cecil, D. J., Doyle, J. D., Kimberlain, T. B., et al. (2017). Rewriting the tropical record books: The extraordinary intensification of Hurricane Patricia (2015). *Bulletin of the American Meteorological Society*, *98*(10), 2091–2112. https://doi.org/10.1175/bams-d-16-0039.1

Sampson, C. R., Fukada, E. M., Knaff, J. A., Strahl, B. R., Brennan, M. J., & Marchok, T. (2017). Tropical cyclone gale wind radii estimates for the Western North Pacific. *Weather and Forecasting*, *32*(3), 1029–1040. https://doi.org/10.1175/waf-d-16-0196.1

Sampson, C. R., Goerss, J. S., Knaff, J. A., Strahl, B. R., Fukada, E. M., & Serra, E. A. (2018). Tropical cyclone gale wind radii estimates, forecasts, and error forecasts for the Western North Pacific. *Weather and Forecasting*, *33*(4), 1081–1092. https://doi.org/10.1175/waf-d-17-0153.1

Sampson, C. R., & Knaff, J. A. (2015). A consensus forecast for tropical cyclone gale wind radii. *Weather and Forecasting*, *30*(5), 1397–1403. https://doi.org/10.1175/waf-d-15-0009.1

Sampson, C. R., & Schrader, A. J. (2000). The automated tropical cyclone forecasting system (version 3.2). *Bulletin of the American Meteorological Society*, *81*(6), 1231–1240. https://doi.org/10.1175/1520-0477(2000)081<1231:tatcfs>2.3.co;2

Sampson, C. R., Schumacher, A. B., Knaff, J. A., DeMaria, M., Fukada, E. M., Sisko, C. A., et al. (2012). Objective guidance for use in setting tropical cyclone conditions of readiness. *Weather and Forecasting*, *27*(4), 1052–1060. https://doi.org/10.1175/waf-d-12-00008.1

Sampson, C. R., Wittmann, P. A., & Tolman, H. L. (2010). Consistent tropical cyclone wind and wave forecasts for the US Navy. *Weather and Forecasting*, *25*(4), 1293–1306. https://doi.org/10.1175/2010waf2222376.1

Sanford, T. B., Price, J. F., Girton, J. B., & Webb, D. C. (2007). Highly resolved observations and simulations of the ocean response to a hurricane. *Geophysical Research Letters*, *34*(13). https://doi.org/10.1029/2007gl029679

Shay, L., & Brewster, J. (2010). Oceanic heat content variability in the Eastern Pacific Ocean for hurricane intensity forecasting. *Monthly Weather Review*, *138*, 2110–2131. https://doi.org/10.1175/2010MWR3189.1

Shay, L. K., Goni, G. J., & Black, P. G. (2000). Effects of a warm oceanic feature on Hurricane Opal. *Monthly Weather Review*, *128*(5), 1366–1383. https://doi.org/10.1175/1520-0493(2000)128<1366:eoawof>2.0.co;2

Shibata, A. (2002). *Chapter 8: AMSR/AMSR-E sea surface wind speed algorithm* (Vol. 9, p. 2). EORC Bulletin/Technical Report. Retrieved from https://sharaku.eorc.jaxa.jp/AMSR/doc/alg/8_alg.pdf

Shibata, A. (2006). A wind speed retrieval algorithm by combining 6 and 10 GHz data from Advanced Microwave Scanning Radiometer: Wind speed inside hurricanes. *Journal of Oceanography*, *62*, 351–359. https://doi.org/10.1007/s10872-006-0060-8

Tallapragada, V., Kieu, C., Kwon, Y., Trahan, S., Liu, Q. F., Zhang, Z., & Kwon, I. H. (2014). Evaluation of storm structure from the operational HWRF during 2012 implementation. *Monthly Weather Review*, *142*(11), 4308–4325. https://doi.org/10.1175/mwr-d-13-00010.1

Walker, N. D., Leben, R. R., Pilley, C. T., Shannon, M., Herndon, D. C., Pun, I. F., et al. (2014). Slow translation speed causes rapid collapse of northeast Pacific Hurricane Kenneth over cold core eddy. *Geophysical Research Letters*, *41*(21), 7595–7601. https://doi.org/10.1002/2014gl061584

Wang, Y., & Wu, C. C. (2004). Current understanding of tropical cyclone structure and intensity changes—A review. *Meteorology and Atmospheric Physics*, *87*(4), 257–278. https://doi.org/10.1007/s00703-003-0055-6

Wentz, F. J., Gentemann, C., Smith, D., & Chelton, D. (2000). Satellite measurements of sea surface temperature through clouds. *Science*, *288*(5467), 847–850. https://doi.org/10.1126/science.288.5467.847

Wu, C. C., Lin, P. H., Aberson, S., Yeh, T. C., Huang, W. P., Chou, K. H., et al. (2005). Dropwindsonde observations for typhoon surveillance near the Taiwan Region (DOTSTAR)—An overview. *Bulletin of the American Meteorological Society*, *86*(6), 787–790.

Wu, C. C., Tu, W. T., Pun, I. F., Lin, I. I., & Peng, M. S. (2016). Tropical cyclone-ocean interaction in Typhoon Megi (2010), a synergy study based on ITOP observations and atmosphere-ocean coupled model simulations. *Journal of Geophysical Research: Atmospheres*, *121*(1), 153–167. https://doi.org/10.1002/2015jd024198

Yang, Y. J., Chang, M. H., Hsieh, C. Y., Chang, H. I., Jan, S., & Wei, C. L. (2019). The role of enhanced velocity shears in rapid ocean cooling during Super Typhoon Nepartak 2016. *Nature Communications*, *10*. https://doi.org/10.1038/s41467-019-09574-3

Yueh, S., Fore, A., Tang, W., Hayashi, A., Stiles, B., Reul, N., et al. (2016). SMAP L-band passive microwave observations of ocean surface wind during severe storms. *IEEE Transactions on Geoscience and Remote Sensing*, *54*, 7339–7350. https://doi.org/10.1109/TGRS.2016.2600239

Zhang, J. A., Cione, J. J., Kalina, E. A., Uhlhorn, E. W., Hock, T., & Smith, J. A. (2017). Observations of infrared sea surface temperature and air-sea interaction in Hurricane Edouard (2014) Using GPS dropsondes. *Journal of Atmospheric and Oceanic Technology*, *34*(6), 1333–1349. https://doi.org/10.1175/Jtech-D-16-0211.1

Zhang, Z., Wang, Y. Q., Zhang, W. M., & Xu, J. (2019). Coastal ocean response and its feedback to typhoon Hato (2017) over the South China Sea: A numerical study. *Journal of Geophysical Research: Atmospheres*, *124*(24), 13731–13749. https://doi.org/10.1029/2019jd031377